Electronic Supplementary Material (ESI) for Nanoscale.

Supplementary information: Observation of different Li intercalation states and local doping in epitaxial mono- and bilayer graphene on SiC(0001)

Wei Huang, Jeong Ah Seo, Mark P. Canavan, Pietro Gambardella, and Sebastian Stepanow*

Department of Materials, ETH Zurich, 8093 Zurich, Switzerland

E-mail: sebastian.stepanow@mat.ethz.ch

Detailed characterizations of Li intercalation

Fig. S1 shows a series of STM images demonstrating the evolution of the epitaxial graphene on SiC(0001) for increasing Li coverage and the post-deposition annealing at room temperature in ultra-high vacuum. Type 0 clusters are easily found within the MLG immediately after the Li deposition in Fig. S1(a). The phase transition from Type 0/MLG to Type 1 is captured at one specific MLG/BLG interface as shown in Fig. S1(b). At the same time, fewer Type 0/MLG clusters are observed within the MLG region. This tendency is more clear with the large-scale scans in Fig. S1(c) where a smooth Type 1 boundary line separates the regions of MLG and BLG. The preferences for the MLG intercalation are interpreted considering the Li diffusion barrier and the adsorption energy. The similar spacing of buffer layer under MLG and buried MLG under BLG[1] facilitates free diffusion of Li atoms with a small diffu-

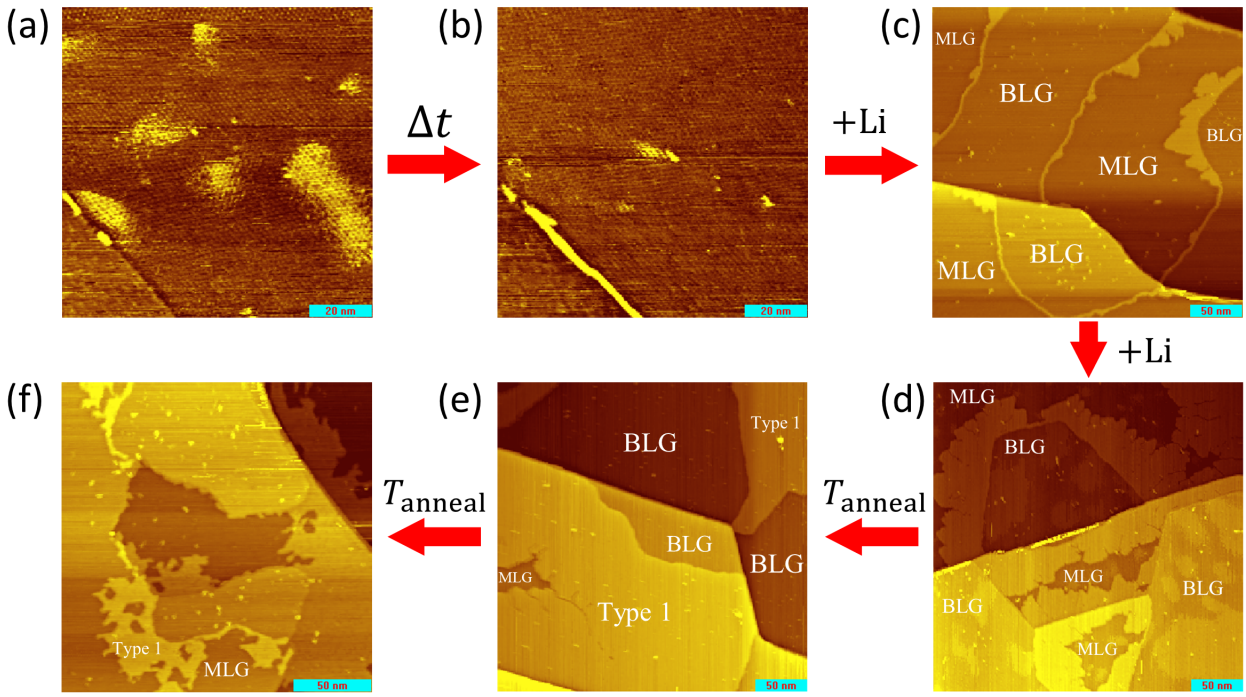

Figure S1: (Color online) (a,b) 100×100 nm STM images of Li-intercalated graphene at the same MLG/BLG interface (a) 2 min and (b) 65 hours after Li deposition. The sample is continuously scanned between two images. Type 0 clusters disappear over time, instead, Type 1 appears as a sharp line at the interface. (c) 300×300 nm large-scale STM images of Li-intercalated graphene with slightly higher coverage. Type 1 lines are now filling the MLG/BLG interfaces and grow inwards in the MLG regions whereas the BLG regions are free of any intercalation. (d,e) 300×300 nm STM images of Li-intercalated graphene after largely increased Li coverage and a subsequent gentle annealing (5 min at around 120 °C). (d) Type 0/BLG clusters appear together with almost filled MLG regions by Type 1 (e). After heating, clean terraces on SiC are observed everywhere implying the complete removal of Type 0 clusters from both MLG and BLG regions. A large domain of Type 1 is identified in (e) from the irregular boundaries inside MLG. (f) 200×200 nm STM images of the Li-intercalated surface after 5 min annealing at around 300 °C. Image conditions: (a,b,e,f) V_{bias}=500 mV, (c) V_{bias}=-250 mV, (d) V_{bias}=100 mV, I_{t}=500 pA for all scans. STM performed at room temperature.

sion barrier on graphene ($<$ 300 meV).[2,3] In fact, the ultrafast Li diffusion between graphene layers has been highlighted by experimental research.[4,5] Simulations predict the dependence of the Li diffusion barrier on the Li concentration x (Li_xC_6),[2] this indicates a different diffusion scenario for the sandwiched Li above buffer layer and buried MLG due to the different chemical and structural nature of buffer layer and MLG.[6,7] Additionally, the adsorption energy of Li on the buffer layer is around 0.9 eV, higher than on graphene (roughly 0.86 eV).[7] Possibly, the local structural defects in the buffer layer are concentrated at interfaces, from where the Li penetration process, as well as the phase transition to Type 1, begins. The width of Type 1 appears to be irregular in the MLG regions. Besides, there is no clear Type 1 accumulation at the SiC steps as well as in the BLG regions. The bright spots in BLG arise from pre-existing imperfections in the pristine graphene growth. The intercalation in the BLG appears after further increasing the Li coverage in Fig. S1(d). The middle regions on the upper terrace represent the BLG regions surrounded by Type 1 stripes at MLG/BLG interfaces, where few clusters are identified as Type 0/BLG. There are some Type 0/MLG clusters visible at the lower terrace as well. Type 0 clusters within the BLG area are only observed after the complete occupation of Type 1 at MLG/BLG interfaces, which block the diffusion entrances towards the MLG region. Li remains between two graphene layers and takes longer to penetrate the graphene beneath due to a higher penetration barrier than the buffer layer. A slight heating results in Li depletion of Type 0/BLG from experimental observations. Eventually, no Type 1 features on the BLG region are detected. Interestingly, all Type 0 clusters disappear after gentle annealing at around 120 °C in Fig. S1(e) while Type 1 regions remain continuous and flat. The situation is disturbed by even higher annealing at around 300 °C as shown in Fig. S1(f), leaving a porous Type 1 region. Clearly, the Li atoms are depleted from the SiC substrate due to the high-temperature heating.

Using STM scans, we monitor spontaneous changes resulting from Li intercalation at the same position on the epitaxial graphene as shown in Fig. S2. Initially, Type 0 clusters mainly occupy MLG regions as seen in Fig. S2(a), but after 16 hours, a clear phase transition from

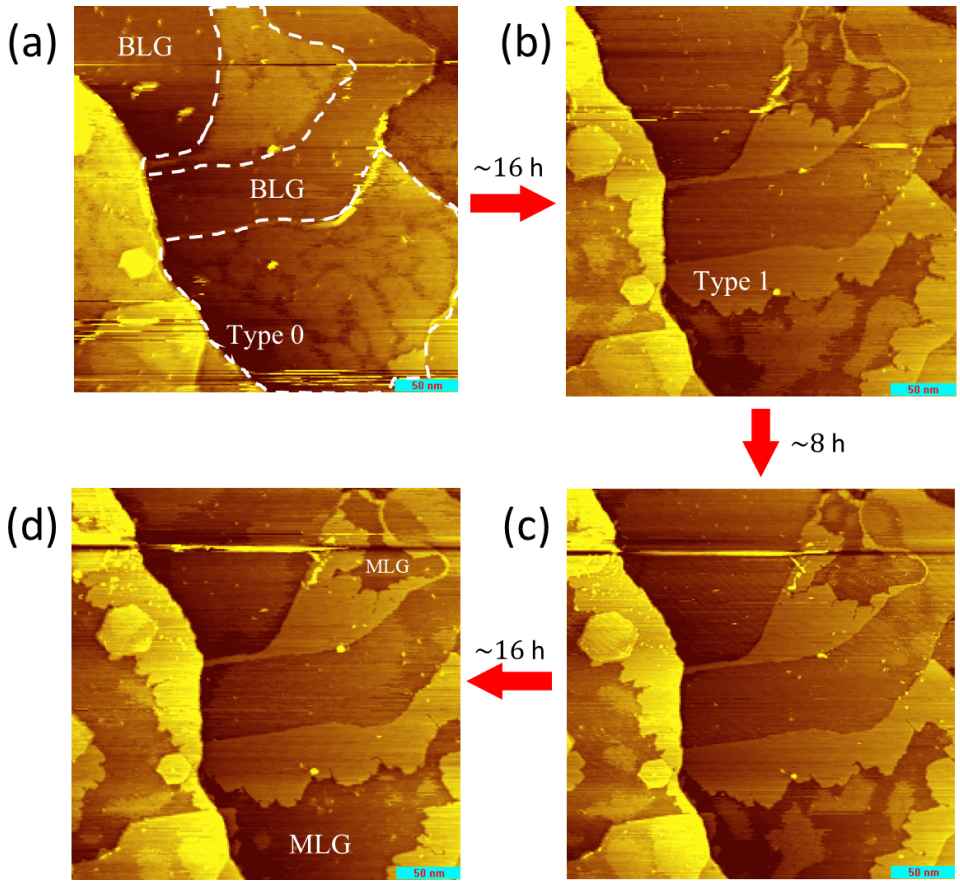

Figure S2: 300×300 nm sequence of STM images of epitaxial graphene after a high dosage of Li deposition. (a) Two MLG patches, where Type 0 clusters almost fully occupy both areas, are encircled with dashed white lines. Some neighboring BLG areas can be found on the same terrace. (b) After 16 hours of scans, the same area shows clear formations of Type 1 stripes near the MLG-BLG interfaces inside the MLG patches. The coexistence of Type 0 and Type 1 within the MLG regions is also observed. (c) The size of Type 0 clusters within MLG regions continues to shrink, while wider Type 1 strips form, as seen in the images taken 8 hours after (b). (d) After 40 hours from the initial Li deposition, the transition from Type 0 to Type 1 is almost complete inside the MLG regions. Image conditions: V_{bias}=500 mV, I_{t}=500 pA for all scans. STM performed at room temperature.

Type 0 to Type 1 is observed at the MLG-BLG interfaces in Fig. S2(b). The growth of Type 1 stripes and the depletion of Type 0 clusters within the MLG regions continues after another 8 hours in Fig. S2(c). Eventually, after 40 hours, the transition is close to completion and the large areas of MLG are surrounded by Type 1 stripes as shown in Fig. S2(d). The area of the Li intercalation decreased by approximately 26% while comparing the same upper MLG region in Fig. S2(a) and Fig. S2(d), indicating that the Li concentration in Type 0 is around 1.35 times lower than in Type 1.

Suppressing bulk conduction in Au-contacted epitaxial graphene on SiC

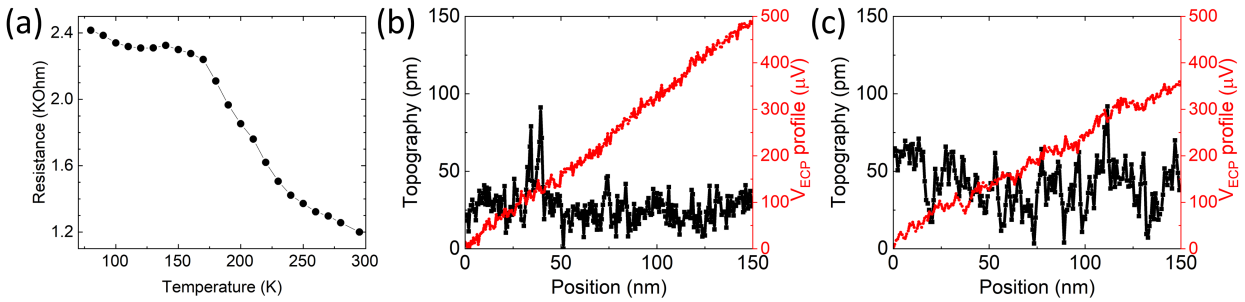

Figure S3: (Color online) (a) Two-point resistance across the Au-contacted epitaxial graphene on SiC versus the sample temperature. The STP measurements are performed at 91 K, with a 4 A/m current density applied through the Au contacts. 5-lines averaged profiles of the electrochemical potential (ECP=eV_{ECP}) and the corresponding topography is extracted from (b) monolayer and (c) bilayer graphene regions. The averaging time to measure the local potential is set to 40 ms per point for one current direction. The slope difference in the V_{ECP} measured in the two different regions imply different local sheet resistance.

After depositing 50 nm thick Au contacts on the epitaxial graphene, the injected current through the contacts can also pass through the SiC bulk, not only through the graphene on top. This strongly reduces the measured potential drop $\Delta V_{\mathrm{ECP}}/\Delta x$. To resolve this issue, the sample is cooled down to liquid nitrogen temperature to increase the SiC bulk resistance substantially. At the same time, it is known that the resistance of graphene decreases only

little compared to RT. This ensures that the sample conductivity is primarily due to the graphene sheet, as shown in Fig. S3(a). To obtain accurate local sheet resistance values, we conduct large-scale ECP maps and then extract local profiles to fit the potential slope $\Delta V_{ECP}/\Delta x$. The sheet resistance is calculated as $\Delta V_{ECP}/(j\Delta x)$, where $j = 4$ A/m is the injected current density in graphene. Fig. S3(b)(c) shows 5-lines averaged profiles of MLG and BLG topography as well as the corresponding ECP data. Clearly, MLG has a higher sheet resistance compared to BLG with the calculated respective resistances being $820\pm3.5\ \Omega$ and $580 \pm 3.5\ \Omega$, respectively.

Analysis of doping and strain in Li-intercalated graphene using Raman spectroscopy

To analyze the quality of the graphene films and the modifications of the strain and doping due to Li intercalation we performed Raman spectroscopy. All Raman spectra were measured with a commercial Horiba Raman (LabRAM HR Evolution UV-VIS-NIR) microscope with a x100 objective, and a Nd:Yag laser with a wavelength of 532 nm. The laser was focused to a spot size of approximately 2 µm diameter with a power of 9.6 mW. To check for local homogeneity and for data averaging we acquired 2D maps in a 120×30 µm rectangle with points spaced by 15 µm in both the x and y direction leading to a total of 27 spatial points per map.

Figure S4 shows the Raman data obtained for the pristine mixed MLG-BLG sample together with the data acquired for the same sample with Li intercalation. The sample with Li intercalation was first measured 24 hours after the Li deposition and should contain a mixture of Type 0 and Type 1 phase. It cannot be stated with certainty that Type 0 phase was present during the Raman measurements since in the STM images after the Raman measurements the Type 0 phase was no longer observed. The sample was measured again after 4 days and some slight annealing which should lead to Type 1 phase only. Fig. S4(a)

shows the full range of Raman frequencies for the different samples including a SiC substrate for comparison and background subtraction that was annealed below the graphitization temperature. In the spectral range shown in Fig. S4(a) graphene exhibits three distinct Raman bands; the D ($\sim$ 1350 cm^{-1}), G ($\sim$ 1600 cm^{-1}), and 2D ($\sim$ 2750 cm^{-1}) which originate from defect-induced, Γ-point, and double-resonant Raman scattering processes, respectively. The G and 2D peaks have pronounced intensities whereas the D band shows no significant contribution with respect to the background. This indicates a good quality of the epitaxial graphene.

In Fig. S4(b) we plot the correlated peak positions of the G and 2D peak as obtained from background subtracted Raman spectra shown in Fig. S4(c) and (d), respectively. The positions of the G and 2D peaks as well as the full width half maximum (FWHM) of the 2D peak are summarized in table 1. We further analyzed the 2D peak width to obtain the layer number N by using the formula[8]

$$N = \frac{45 \text{ cm}^{-1}}{88 \text{ cm}^{-1} - \text{FWHM(2D)}} \,. \tag{1}$$

The thus obtained number of graphene layers are also reported in table 1. For the pristine graphene we find $N = 1.4 \pm 0.3$, i.e., we have mostly (60%) MLG with some patches (40%) of BLG. The observed positions for the Raman G and 2D bands match previous observations.[8,9] The Raman shifts corresponds to strained graphene with a compressive strain of about -0.4% and an electron doping level of $1 \cdot 10^{13}$ cm^{-2}. The small deviations of our data from the ones reported in Refs.[8,9] are ascribed to a layer number of $N > 1$ in our work.

Upon Li intercalation, we observe a clear redshift of the G and 2D Raman bands without the formation split peaks in the Raman spectrum, which indicates a homogeneous Li intercalation scenario. We observe only small differences in the two Li intercalation samples where the G band shifts to about 1592 cm^{-1} by -9 cm^{-1} and the 2D peak by about -34 cm^{-1} to 2716 cm^{-1} for the data acquired 24 hours after Li intercalation. The apparent

layer number has increased to 1.55 ± 0.1 but the increased width of the 2D peak could be also due to inhomogeneities in the sample. The peak positions are very similar for the data measured 4 days after Li intercalation but show a further increase in the layer number to $N = 1.8 \pm 0.1$ which is in line with the conversion of MLG to a quasi free BLG (Type 1) upon Li intercalation. Apart from the peak shifts also the intensities and intensity ratios between the G and 2D peak are modified. While the ratio $I(2D)/I(G)$ is 1.6 for the pristine and 24h Li sample it increased to about 2.2 for the 4d Li sample. We do not have an explanation for this behavior since an increased intensity ratio is associated with a reduced layer number whereas we expect a conversion form the MLG to a quasi free BLG upon the formation of Type 1 phase.

The phonon frequencies in graphene can be shifted by strain and carrier concentration.[9,11,12] The strain and doping induced shifts of the G and 2D frequencies can be quantified where one assumes the two sources to be independent from each other and that their induced shifts can be added linearly. The Raman peak shift can be expressed by the following relationship

$$\omega_i = \omega_i^0 + \Delta\omega_i^s + \Delta\omega_i^d \tag{2}$$

where ω_i is the resultant (measured) Raman frequency of the i = G or 2D band, ω_i^0 is the Raman band frequency of unstrained and undoped graphene, $\Delta\omega_i^s$ is the induced shift due to mechanical strain, and $\Delta\omega_i^d$ is the induced shift due to carrier doping. The unstrained and undoped graphene Raman frequencies are shown as a green dot in Fig. S4(b) as obtained from Refs.[10,11] A dashed line shows how the Raman shifts behave under biaxial strain,[11] where positive shifts with respect to the unstrained/undoped graphene mean compressive strain. For biaxial strain the correlated shifts are about $\Delta\omega_{2D}^s/\Delta\omega_G^s = 2.6 \pm 0.2$.[11] Regarding the doping, we consider here only electron doped graphene for which non-monotonic shifts of the G and 2D bands were found.[12] With increasing electron concentration the G peak shifts up in frequency almost linearly until the Fermi energy of 0.8 eV, however, the 2D band remains nearly the same until a Fermi energy of 0.6 eV and then goes quickly to lower frequencies

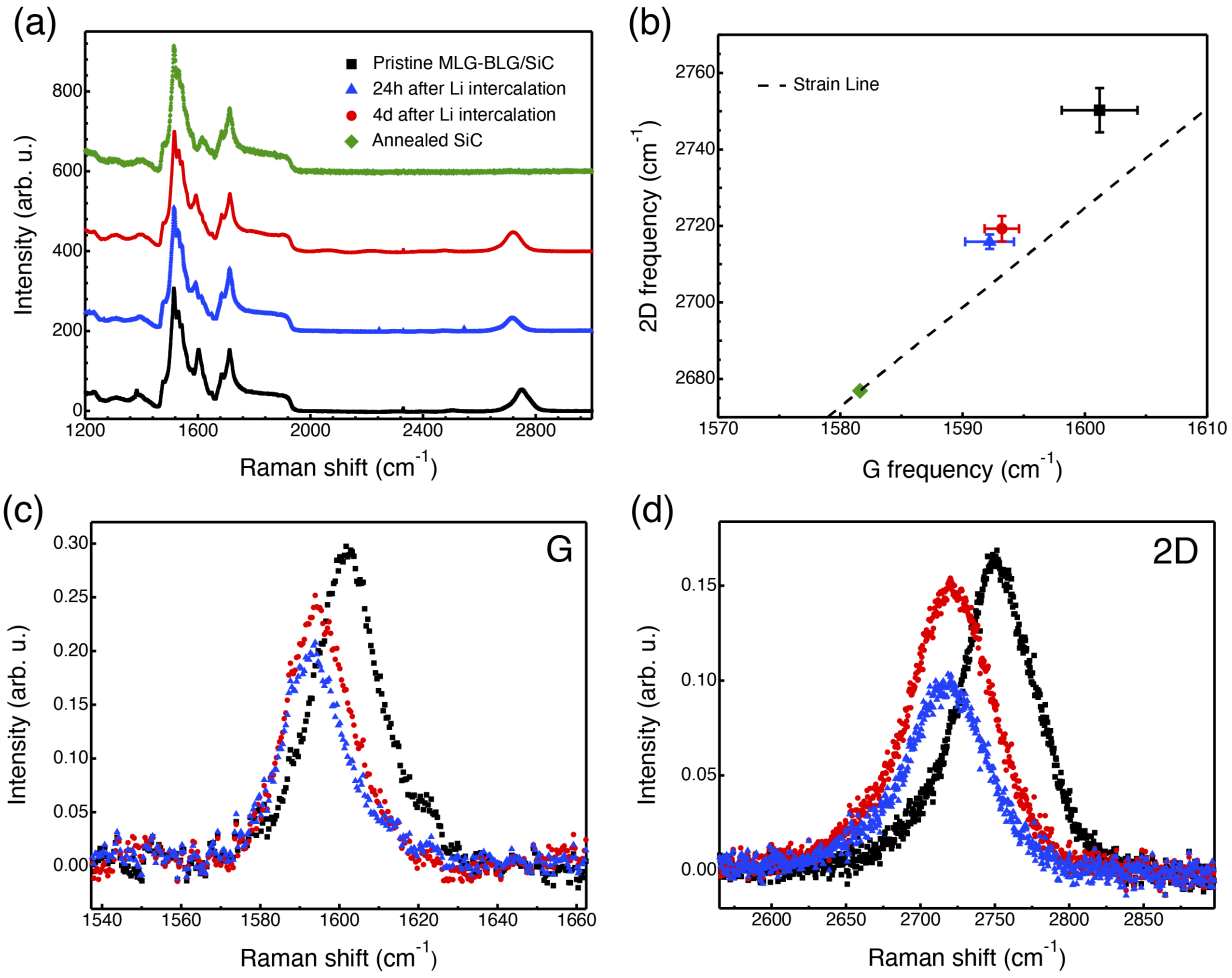

Figure S4: (Color online) (a) Raman data for graphene before and after Li intercalation and at different stages after Li intercalation. For comparison the Raman data acquired for annealed SiC (temperature below graphitization) is also shown and used for background subtraction. (b) Correlated G and 2D peak positions for the different samples. The green dot marks unstrained and undoped graphene as found in literature.[10,11] The dashed line marks the expected behavior for graphene under biaxial strain.[11] (c) Background subtracted G band. (d) Background subtracted 2D band.

when increasing the Fermi energy to 0.8 eV. A correction that has to be considered is that our data acquired at 532 nm should red shift with respect to data acquired at 514 nm in Refs.[11,12] by 7.6 cm^{-1}.[9]

Table 1: Position of G and 2D peaks and FWHM of 2D peak (all in cm^{-1}) with calculated layer numbers as obtained from a peak fit with a single Lorentzian of the background subtracted data.

	pristine	Li (24 hours)	Li (4 days)
G position	1601.2 ± 3.1	1592.2 ± 2.0	1593.2 ± 1.4
2D position	2750.3 ± 5.8	2715.9 ± 1.9	2719.3 ± 3.3
Number of layers	1.41 ± 0.34	1.55 ± 0.08	1.79 ± 0.12
2D FWHM	54.7 ± 5.7	58.9 ± 1.5	62.8 ± 1.8

In our data the redshift of the G peak for the Li intercalated sample goes against an increased electron doping which would shift the G peak to higher frequencies. Hence, the Li intercalation must lead to a much reduced compressive strain. An increase of the Fermi energy from 0.5 eV to 0.8 eV for the Type 1 phase emerging from MLG should lead to a G peak shift of about 10 cm^{-1} to higher frequencies.[12] At the same time the 2D peak should shift to lower frequencies by about 30 cm^{-1}. Thus, the Raman shifts for the Li intercalated graphene with predominant Type 1 phase indicates that the compressive strain was reduced roughly by a factor 2. A full quantitative analysis is hindered by the presence of mixed MLG and BLG domains in the pristine graphene sample.

The small difference between the 24h and 4d Li data is ascribed to the presence of only little Type 0 phase after taking the sample out of vacuum for Raman measurements. It is also not clear if the Li intercalated graphene is stable in air despite the fact that the samples measured in STM after the Raman measurements without any annealing did not exhibit any direct sample modification apart from the absence of any mobile Type 0 phase. Also the laser used for the Raman measurements could accelerate the transition from Type 0 to Type 1 phase.

We conclude that the Li intercalation yielding to the Type 1 phase results in clear shifts of the Raman G and 2D bands that are consistent with a reduction of the compressive strain

and an increase in electron doping but the analysis is further complicated by a possible sample inhomogeneity due to presence of MLG and BLG patches and a change in layer number upon Li intercalation. The apparent large strain values obtained from the STM topographs of the Type 0 phase could not be confirmed in the Raman measurements which is ascribed to an instability of the phase in air or during the Raman measurements.

STM topographs for STS data

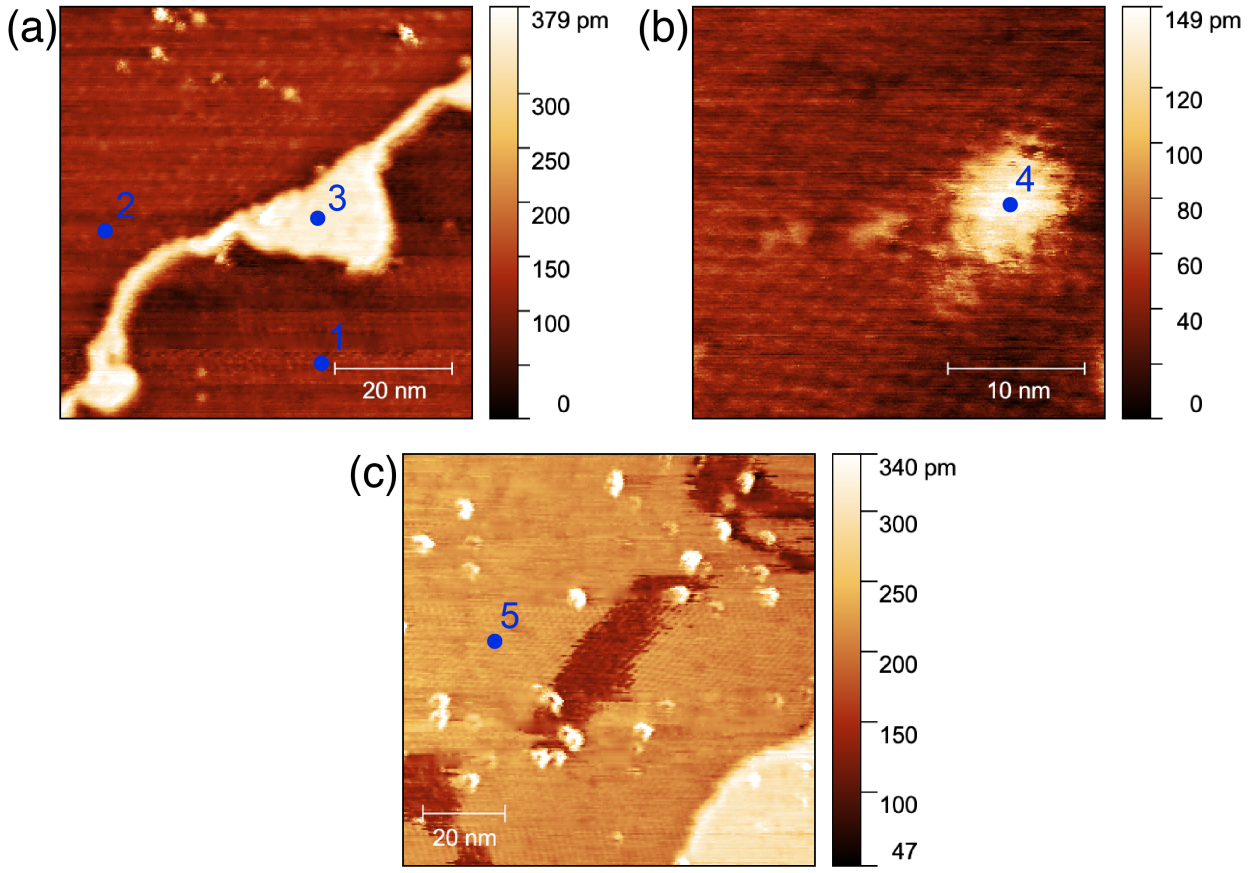

Figure S5: (Color online) (a-c) STM topographs from samples with different Li content on which the STS data in Fig. 3 was obtained. The blue dots mark the positions where the STS was acquired: 1 - MLG, 2 - BLG, 3 - Type 1, 4 - Type 0/MLG, 5 - Type 0/BLG.

References

(1) Huang, H.; Chen, W.; Chen, S.; Wee, A. T. S. Bottom-up growth of epitaxial graphene on 6H-SiC (0001). *ACS nano* **2008**, *2*, 2513–2518.

(2) Persson, K.; Hinuma, Y.; Meng, Y. S.; Van der Ven, A.; Ceder, G. Thermodynamic and kinetic properties of the Li-graphite system from first-principles calculations. *Physical Review B* **2010**, *82*, 125416.

(3) Shtepliuk, I.; Yakimova, R. Interaction of H and Li with epitaxial graphene on SiC: A comparative analysis by first principles study. *Applied Surface Science* **2021**, *568*, 150988.

(4) Kühne, M.; Paolucci, F.; Popovic, J.; Ostrovsky, P. M.; Maier, J.; Smet, J. H. Ultrafast lithium diffusion in bilayer graphene. *Nature nanotechnology* **2017**, *12*, 895–900.

(5) Kühne, M.; Börrnert, F.; Fecher, S.; Ghorbani-Asl, M.; Biskupek, J.; Samuelis, D.; Krasheninnikov, A. V.; Kaiser, U.; Smet, J. H. Reversible superdense ordering of lithium between two graphene sheets. *Nature* **2018**, *564*, 234–239.

(6) Kim, S.; Ihm, J.; Choi, H. J.; Son, Y.-W. Origin of anomalous electronic structures of epitaxial graphene on silicon carbide. *Physical Review Letters* **2008**, *100*, 176802.

(7) Li, Y.; Zhou, G.; Li, J.; Wu, J.; Gu, B.-L.; Duan, W. Lithium intercalation induced decoupling of epitaxial graphene on SiC (0001): Electronic property and dynamic process. *The Journal of Physical Chemistry C* **2011**, *115*, 23992–23997.

(8) Lee, D. S.; Riedl, C.; Krauss, B.; Von Klitzing, K.; Starke, U.; Smet, J. H. Raman spectra of epitaxial graphene on SiC and of epitaxial graphene transferred to SiO_2. *Nano Letters* **2008**, *8*, 4320–4325.

(9) Schmidt, D. A.; Ohta, T.; Beechem, T. E. Strain and charge carrier coupling in epitaxial graphene. *Physical Review B* **2011**, *84*, 235422.

(10) Graf, D.; Molitor, F.; Ensslin, K.; Stampfer, C.; Jungen, A.; Hierold, C.; Wirtz, L. Spatially resolved Raman spectroscopy of single- and few-layer graphene. *Nano Letters* **2007**, *7*, 238–242.

(11) Lee, J. E.; Ahn, G.; Shim, J.; Lee, Y. S.; Ryu, S. Optical separation of mechanical strain from charge doping in graphene. *Nature Communications* **2012**, *3*, 1–8.

(12) Das, A.; Pisana, S.; Chakraborty, B.; Piscanec, S.; Saha, S. K.; Waghmare, U. V.; Novoselov, K. S.; Krishnamurthy, H. R.; Geim, A. K.; Ferrari, A. C.; Sood, A. K. Monitoring dopants by Raman scattering in an electrochemically top-gated graphene transistor. *Nature Nanotechnology* **2008**, *3*, 210–215.